Growth of Aligned Single-Crystalline Rutile TiO2 Nanowires on Arbitrary Substrates and Their Application in Dye-Sensitized Solar Cells

ARTICLE *in* THE JOURNAL OF PHYSICAL CHEMISTRY C · APRIL 2010

Impact Factor: 4.77 · DOI: 10.1021/jp100491h

3 AUTHORS, INCLUDING:

Akshay Kumar

9 PUBLICATIONS **880** CITATIONS

SEE PROFILE

Anuj R. Madaria

University of Southern California

9 PUBLICATIONS **583** CITATIONS

SEE PROFILE

Growth of Aligned Single-Crystalline Rutile TiO_2 Nanowires on Arbitrary Substrates and Their Application in Dye-Sensitized Solar Cells

Akshay Kumar, Anuj R. Madaria, and Chongwu Zhou*

Department of Electrical Engineering and Center for Energy Nanoscience and Technology, University of Southern California, Los Angeles, California 90089

Received: January 18, 2010; Revised Manuscript Received: March 22, 2010

TiO_2 is a wide band gap semiconductor with important applications in photovoltaic cells and photocatalysis. In this paper, we report synthesis of single-crystalline rutile phase TiO_2 nanowires on arbitrary substrates, including fluorine-doped tin oxide (FTO), glass slides, tin-doped indium oxide (ITO), Si/SiO_2, Si(100), Si(111), and glass rods. By controlling the growth parameters such as growth temperature, precursor concentrations, and so forth, we demonstrate that anisotropic growth of TiO_2 is possible leading to various morphologies of nanowires. Optimization of the growth recipe leads to well-aligned vertical array of TiO_2 nanowires on both FTO and glass substrates. Effects of various titanium precursors on the growth kinetics, especially on the growth rate of nanowires, are also studied. Finally, application of vertical array of TiO_2 nanowires on FTO as the photoanode is demonstrated in dye-sensitized solar cell with an efficiency of $2.9 \pm 0.2\%$.

Introduction

Synthesis of metal oxide materials has been an area of extensive research owing to their widespread applications.[1] In the past two decades, there have been great efforts in synthesizing one-dimensional (1-D) metal oxide nanowires because of their unique shape-dependent electronic and optical properties.[2−11] Among others, ZnO and TiO_2 are of particular interest because of their demonstrated applications in a wide variety of commercial products including pigment,[12] sunscreens,[13] paints,[14] ointments, protective coating, and so forth.[15] Advances in synthetic chemistry techniques have allowed alteration and manipulation of the magnetic and electrical properties of these materials by introducing doping impurities into the lattice.[16,17] TiO_2 has also been one of the most significant materials for photocatalysis and photovoltaics applications. The extraordinary oxidizing ability of photogenerated holes in TiO_2 together with its relative chemical and physical stability has made TiO_2 a material of choice for applications related to solar energy such as dye-sensitized solar cell (to convert light into electricity),[18−20] photoelectrolytic hydrogen generation,[21] and UV-mediated photocatalysis.[22] The motivation behind synthesizing 1-D metal oxide materials has come from the fact that their 1-D shape results in the appearance of new optical and electrical properties which make them all the more beneficial for the above-mentioned usage.

However, while ZnO has seen much advance in synthesizing nanowires, synthesis techniques for TiO_2 nanowires are limited. For example, vertical arrays of ZnO nanowires have been grown using a simple solution method on a variety of substrates including tin-doped indium oxide (ITO), fluorine-doped tin oxide (FTO), silicon, glass, and polyethylene terephthalate (PET) substrates.[23] This partly comes from the fact that ZnO possesses a wurtzite crystal structure with six nonpolar {1010} faces and rather unstable {0001} polar faces which suggests a growth habit where the *c*-axis is the fastest growing direction.[24] Unlike ZnO, TiO_2 has witnessed limited progress toward a low-temperature synthesis protocol allowing for its growth on arbitrary substrates. There have been reports on TiO_2 nanowire growth utilizing heterogeneous nucleation based on vapor−liquid−solid (VLS) techniques, but they typically require very high growth temperatures.[25−27] In the past, while the anodization method has been used to grow TiO_2 nanotubes,[28] an oblique angle deposition method has been demonstrated for TiO_2 nanowire growth.[29] Very recently, TiO_2 nanowires using hydrothermal[30] and solvothermal[31] methods were synthesized, but the growth was reported to be restricted to FTO substrate, and attempts to grow nanowires on glass or silicon substrates were not successful.[30] In this paper, we report a general synthesis procedure which allows growth of TiO_2 nanowires on arbitrary substrates including FTO, glass slides, ITO, Si/SiO_2, Si(100), and Si(111) substrates. We further demonstrate that a densely packed vertical array of TiO_2 nanowires can be grown directly on glass slide as well by controlling the substrate position. In addition, we have used vertical array of TiO_2 nanowires grown on FTO substrate as photoanode to assemble a dye-sensitized solar cell with an efficiency of 2.9%. The growth of TiO_2 nanowires on arbitrary substrates can catalyze many more applications such as Li-ion battery and water splitting, which may require substrates other than FTO.

Experimental Details

Synthesis of TiO_2 Nanowires. TiO_2 nanowire assemblies were grown on various substrates including FTO, glass slides, ITO, Si/SiO_2, Si(100), and Si(111) substrates. In a typical synthesis, the substrate was ultrasonically cleaned sequentially in acetone, isopropyl alcohol (IPA), and deionized (DI) water for 15 min each and was finally dried under N_2 flow. Separately, 1 mL of a titanium precursor was added dropwise to a 1:1 mixture of DI water and concentrated (35%) hydrochloric acid (HCl) to obtain a clear transparent solution. Titanium precursors used in this study include titanium tetrachloride, titanium isopropoxide, and titanium n-butoxide. The substrate was placed at an angle (see text for discussion on the effect of substrate placement angle) in a 23 mL Teflon liner, and the precursor solution was added to it. The Teflon liner was loaded in an

* To whom correspondence should be addressed. E-mail: chongwuz@usc.edu.

10.1021/jp100491h
Published on Web 04/14/2010

autoclave and was placed in an oven, and the growth was carried out at different temperatures (120−180 °C) and for different growth times (2−8 h). Detailed synthesis conditions are discussed at appropriate places in the text. In our approach, the titanium precursor concentration in the reaction solution is 3 times higher than that used in previous work,[30] which led to the significantly different results discussed below.

Solar Cell Fabrication. For the fabrication of dye-solar cell, an FTO substrate with vertical array of nanowires was immersed in 0.3 mM ethanolic solution of *cis*-bis(isothiocyanato)bis(2,2′-bipyrridyl-4-4′-dicarboxylato)-ruthenium(II)bis-tetrabutylammonium dye (N-719 as received from Solaronix) for 12−24 h, which serves as the light-absorbing elements. A 20 nm platinum-coated FTO substrate was used as the counter electrode. A sheet of parafilm was used as a spacer, and the space between the electrodes was filled with commercially available electrolytic solution (iodyte 100 from Solaronix) by capillary action to complete the cell fabrication. For the $TiCl_4$ treatment, FTO substrate with nanowire array was immersed in 0.1 M solution of $TiCl_4$ (prepared by adding $TiCl_4$ dropwise into the measured amount of ice) at 60 °C for 30 min and subsequently was annealed at 400 °C in air for 30 min.

Characterization. Scanning electron microspcope (SEM) images were obtained on JEOL-7001 SEM operating at 5.0 kV voltage. Powder X-ray diffraction (XRD) analyses were performed on a Rigaku Ultima IV X-ray diffractometer using a Cu Kα radiation source ($\lambda = 1.54$ Å). Transmission electron microscope (TEM) and selected area electron diffraction (SAED) analyses were carried out on a JEOL JEM-2100 microscope at an operating voltage of 200 kV equipped with a Gatan CCD camera. To prepare TEM samples, substrates with as-grown nanowires were sonicated at mild power in IPA solution, and a drop of this solution was put on the 300 mesh Cu grid. Current−voltage characteristics were measured using an Agilent semiconductor parameter analyzer. An Oriel 300 W Xe lamp fitted with AM-1.5G filter was used to simulate the solar spectrum. The sample with an active area of 0.3 cm^2 was illuminated by the light from the Xe lamp, and the corresponding photocurrent and photovoltage generated were measured.

Results and Discussions

Nanowire Growth on Arbitrary Substrates. We synthesized TiO_2 nanowires on various substrates including FTO, ITO, glass (slide and rod), Si/SiO_2, Si(100), and Si(111) and obtained nanowires with slightly different morphologies depending upon the substrate used. Figure 1 shows the field emission scanning electron microscope (FESEM) images of TiO_2 nanowires on (a, b) FTO, (c, d) glass, (e, f) ITO, and (g, h) Si/SiO_2 using $TiCl_4$ as the titanium precursor. Highly aligned array of TiO_2 nanowire array could be grown on an FTO substrate with a length of 6.8 μm when the growth was carried out at 180 °C for 4 h. Nanowires grown in this fashion were ∼100 nm in diameter with a square cross section (Figure 1a inset). Also, the diameter was larger at the bottom and seemed to taper toward the tip. The cross-sectional image shows the highly ordered and aligned array with a very close packing (Figure 1b). The nanowires grew all over the substrate with uniform morphology.

To check the versatility of the growth process, we employed a glass substrate, and remarkably, nanowires grew on the glass substrate as well. This is in contrast with the report of Liu and Aydil[30] where they reported that attempted growth on glass and silicon substrates was not successful. SEM inspections demonstrated that nanowires exhibited dandelion morphology when the substrate was kept horizontal relative to the base of the autoclave (Figure 1c), while nanowires formed vertical array structure when the substrate was loaded vertically (Figure 1d). The effect of substrate positioning will be discussed later in the manuscript. Uniform vertical alignment in the case of FTO can arise from the fact that TiO_2 and FTO have similar crystal structure, which can lead to epitaxial growth of TiO_2 nanowires on FTO.[30] In contrast, there is no lattice match between TiO_2 and the glass substrates, and consequently, the growth on the glass substrate resulted in dandelion-like morphology with ordered nanowires growing on microsized particles. The diameter of the nanowire was found to be ∼90 nm with a length of ∼4 μm. We also employed glass rod and glass tube as the substrate, and nanowires grew all over the substrate with morphologies similar to that on other substrates. Also, when we examined the inner wall of the Teflon cup, we found TiO_2 nanowires on the surface. SEM images of TiO_2 nanowires on the glass rod, glass tube, and inner wall of the Teflon cup are shown in the Supporting Information, SI-1.

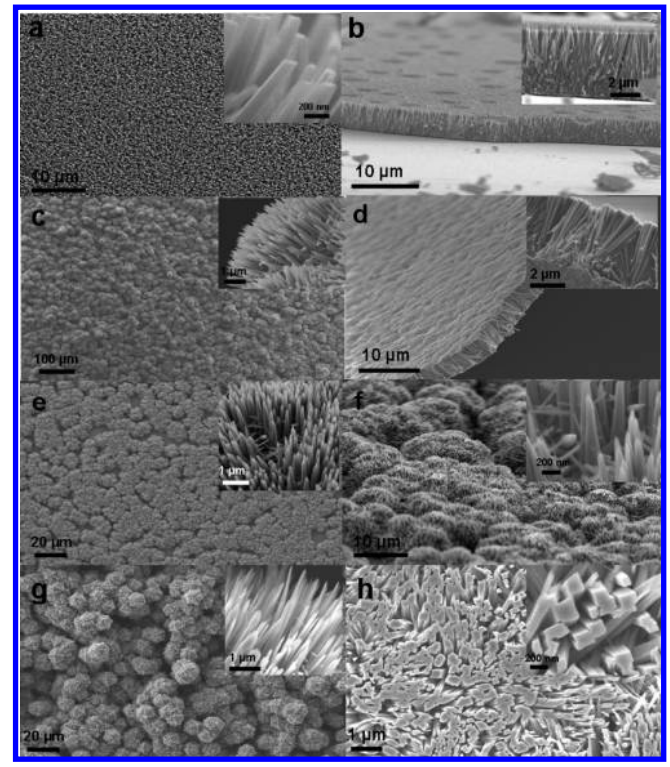

Figure 1. SEM images of TiO_2 nanowires grown using 10 mL of DI water, 10 mL of HCl, and 1 mL of $TiCl_4$ at 180 °C for 4 h on different substrates. (a) FTO substrate, top view. (b) FTO substrate, cross-sectional view. (c) Glass substrate, top view. (d) Glass substrate, perspective view. (e) ITO substrate, top view. (f) ITO substrate, perspective view. (g) Si/SiO_2 substrate, top view. (h) Back side of the TiO_2 film peeled off from the Si/SiO_2 substrate. In every image, the inset shows the corresponding nanowires at higher resolution.

When the growth was carried out on ITO substrates, there was formation of similar dandelion-type structures albeit with comparatively lower density and smaller-sized dandelions (∼20 μm) (Figure 1e and 1f). Individual TiO_2 nanowires grew in radially outward direction on ITO substrate similar to the growth on glass substrate. We further explored the growth of nanowires on Si/SiO_2 (Figure 1g), Si (100), and Si(111) substrates (see Supporting Information, SI-2) and obtained similar dandelion-shaped nanowire assemblies. It was relatively easier to peel off the film of TiO_2 nanowires from Si and Si/SiO_2 substrates than from FTO, ITO, and glass substrates. To find the structure of nanowires at the interface, we carried out SEM imaging on the

TABLE 1: Summary of Different TiO_2 Nanowire Morphologies Obtained on Different Substrates

substrate	morphology	size of dandelion	length	diameter
FTO	vertical array	NA	5.6 μm	~100 nm
ITO	dandelions	~20 μm	4 μm	~80 nm
glass	dandelions	~10−20 μm	3 μm	~80 nm
Si/SiO_2	dandelions	~10−20 μm	3 μm	~90 nm
Si(100)	dandelions	~30−40 μm	4 μm	~90 nm
Si(111)	dandelions	~20 μm	4 μm	~90 nm

peeled-off films. Interestingly, square-shaped individual nanowires with a size of ~200 nm were found at the interface of Si/SiO_2 substrate and the nanowire film (Figure 1h), which suggests that nanowires start to grow from a thin film of TiO_2 deposited on the substrate. The domain size of the dandelions was larger in size (~40 μm) in the case of Si(100) with dandelions merged into each other (Supporting Information, Figure SI-2a). The density of dandelions was low on Si(111) substrate compared to other silicon substrates.

Successful growth of TiO_2 nanowires on substrates such as ITO, glass, Si/SiO_2, and Si, which do not have any epitaxial interface between them and TiO_2, suggests that such an epitaxial interface is not required to grow TiO_2 nanowires, though different substrates apparently led to nanowires of different morphologies and dimensions. In the case of FTO, the epitaxial interface can help the alignment of nanowires, and therefore, uniform vertical array of nanowires was obtained. In contrast, observation of dandelion-shaped morphologies on other substrates suggests that, in the absence of epitaxial interface, TiO_2 first nucleated as islands on these substrates and subsequently grew from these islands to form dandelion-like morphologies. The TiO_2 nanostructure topologies from various substrates are summarized in Table 1.

The nanowires were subsequently characterized using X-ray diffraction (XRD), transmission electron microscope (TEM), and selected-area electron diffraction (SAED). Nanowires grown in this report, regardless of the substrate used, were found to have rutile phase. XRD data (Figure 2a, 2b) show an excellent agreement with the standard rutile structure of TiO_2 (PDF file #01-086-0147, $P4_2/mnm$, $a = b = 4.594$ Å and $c = 2.958$ Å). Figure 2a shows the XRD pattern for nanowires grown on the glass substrate while Figure 2b shows XRD data for nanowires grown on an FTO substrate. A clear difference in the relative intensities of peaks corresponding to various crystallographic planes is visible in Figure 2a and Figure 2b. A sharp increase in the (002) peak intensity (compared to the powder XRD pattern) in the case of FTO substrate indicates that the as-grown nanowire array is highly oriented with respect to the substrate surface. On the other hand, the XRD pattern for the glass substrate exhibits peaks for other reflections as well. However, the intensity of the (002) peak increases from 6.7% of the (110) peak intensity in the standard powder spectrum to 16.3% of the observed (110) peak intensity suggesting preferential growth of nanowires in the [001] direction. TEM measurements confirmed the single crystallinity of the nanowires grown in this fashion. Figure 1c shows the high-resolution TEM (HR-TEM) image of a single nanowire. Lattice planes corresponding to {110} planes are distinctly visible. Spacing based on 10 planes was calculated to be 3.23 Å for the [110] planes. Figure 1d shows a selected-area electron diffraction (SAED) pattern of a single TiO_2 nanowire with $[1\bar{1}0]$ being the zone axis.

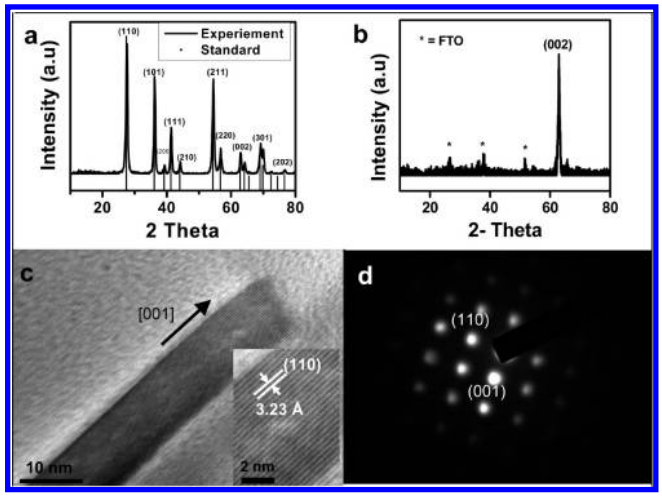

Figure 2. Structural characterization of TiO_2 nanowires grown at 180 °C for 4 h with 10 mL of DI water, 10 mL of HCl, and 1 mL of $TiCl_4$. (a, b) XRD pattern of nanowires grown on the glass and FTO substrate, respectively. (c) TEM image of a single nanowire. Inset shows an HRTEM image of the same nanowire. (d) SAED pattern of a single nanowire.

Both crystalline and amorphous TiO_2 have been synthesized in the past using hydrolysis of $TiCl_4$.[32] It is well-known that when $TiCl_4$ is mixed with water, it undergoes hydrolysis (violent reaction releasing HCl) resulting in the formation of amorphous TiO_2.[32] To obtain crystalline TiO_2, one important factor is to slow down hydrolysis of $TiCl_4$ by providing a highly acidic environment.[33] Addition of HCl inhibits decomposition of $TiCl_4$, which facilitates formation of crystalline TiO_2.[34] Further addition of HCl slows down the reaction to the extent that thermodynamics dictates the growth direction rather than the kinetics as discussed below. Also, rutile structure has a 4_2 screw axis along the crystallographic *c*-axis which promotes the growth along the [001] direction leading to a crystal morphology dominated by the {110} faces.[35,36]

Growth Mechanism. The growth habit of crystals is mainly determined by the relative growth of various crystal faces bounding the crystal, which is dependent on internal structure factors of a given crystal and on external conditions such as temperature, concentration of precursor, pH value of the solution, and so forth. In principle, one can tune the synthesis conditions to allow the system to evolve with minimum surface energy, that is, under conditions that are thermodynamically stable. In case of rutile TiO_2, every Ti atom is bound by six oxygen atoms forming a TiO_6 octahedral which shares a pair of opposite edges with the next octahedral forming a chainlike structure.[37] Depending upon the numbers of corners and edges of the coordination polyhedra available, the growth rate of the different crystal faces differs and follows the sequence (110) < (100) < (101) < (001).[38] The growth of TiO_2 in aqueous solution results from the formation of the growth units and their incorporation into the crystal lattice. The nature of the growth units, which are Ti(IV) complex ions, depends critically on the acidity and ligand in solution. In the present reaction conditions, the formation of TiO_2 might take place according to the following reactions:

$$TiCl_4 + H_2O \rightarrow HCl + \text{Ti(IV) complex}$$

$$2\text{Ti(IV) complex} \xrightarrow{\text{dehydration}} TiO_2$$

The presence of an abundant amount of H^+ from the hydrochloric acid significantly restricts the supply of the growth

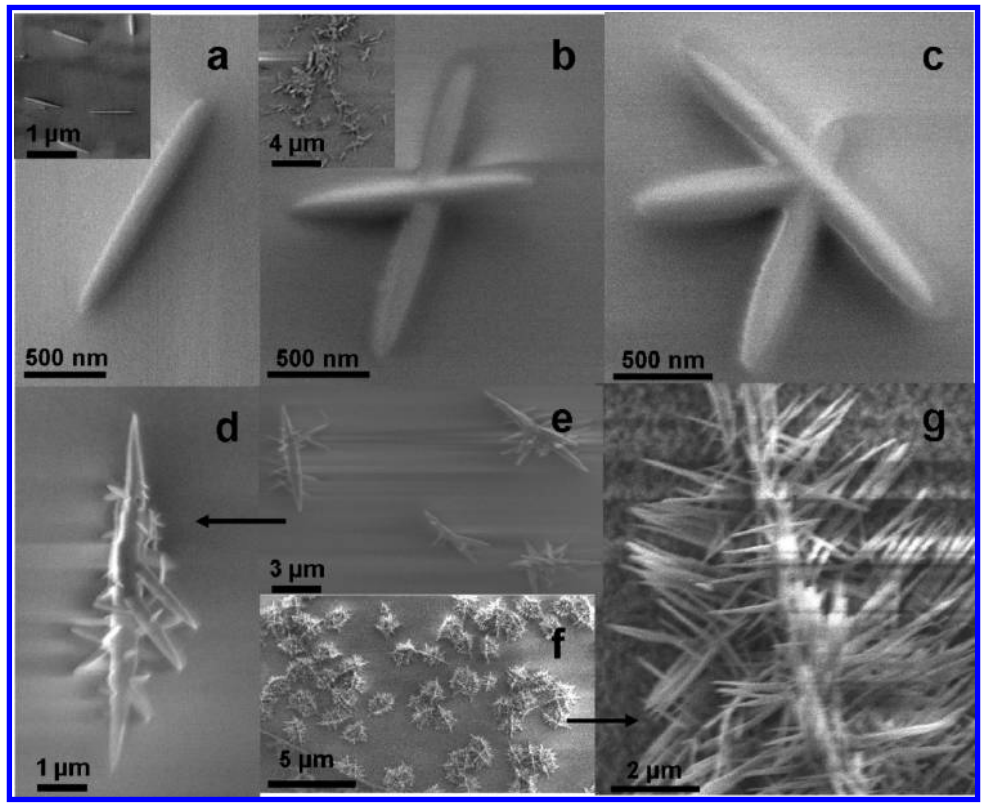

Figure 3. SEM images showing the evolution of nanowire morphology grown using 10 mL of DI water and 10 mL of HCl for 1 h with different amounts of $TiCl_4$ concentration and different temperatures. (a) Individual nanowires obtained using 0.5 mL $TiCl_4$ at 150 °C; inset shows large area image. (b) Crosslike structure and (c) three-leg structures obtained using 0.75 mL $TiCl_4$ at 150 °C; inset shows large area image. (d) Dendrite structure obtained using 1 mL $TiCl_4$ at 150 °C. (e) Large area image of dendritic structures. (f) Large area image of treelike structures. (g) Treelike branched structure obtained using 1 mL $TiCl_4$ at 180 °C.

units, and the morphology is determined by the incorporation mechanism of the growing crystal. As mentioned above, for rutile TiO_2, growth rate in the [001] direction is the highest resulting in the growth of stable *c*-elongated anisotropic crystals exhibiting (110) faces. In addition, the presence of Cl^- ions is known to restrict growth of the (110) faces further enhancing the growth along the (001) direction.[30] Thus, according to the crystal-symmetry and surface-energy considerations, a typical crystal habit should be acicular and tabular and should exhibit a square cross section as shown in the Supporting Information, SI-3.

To understand the growth mechanism, we carried out controlled experiments on ITO substrate. Both the growth temperature and the amount of titanium precursors were varied, and the obtained nanowire morphology was inspected in high-resolution SEM. Figure 3 shows the evolution of the nanowire structure as the growth temperature and the precursor concentration were increased. An amount of 0.5 mL of $TiCl_4$ and a growth temperature of 150 °C for 1 h resulted in the growth of individual nanowires as shown in Figure 3a. The length of the nanowire was 1.5 ± 0.2 μm with a diameter of 100 ± 15 nm in the center and ~60 nm at the ends. Since the substrate used was ITO which has a cubic crystal structure, epitaxial growth of TiO_2 on ITO was not possible. When a higher $TiCl_4$ amount of 0.75 mL was used, many crosslike structures appeared (Figure 3b). In addition to crosslike structures, we also observed three-leg nanowire structures (Figure 3c) although with relatively low proportion. Both individual and branched nanowires were obtained everywhere on the substrate as observed in large area SEM images shown in the insets of Figure 3a and Figure 3b. When an even higher $TiCl_4$ amount of 1 mL was used, many nanowires started to grow from a central long nanowire resulting in a dendritic-like structure as shown in Figure 3d and Figure 3e. We believe that the additional nanowires start to grow at certain planes with incorporation of defects at the interface. When the temperature was increased from 150 to 180 °C, keeping the $TiCl_4$ amount at 1 mL, the growth resulted in tree-shaped structures with many nanowires growing on a central wire (Figure 3f and Figure 3g).

Since the hydrolysis rate of titanium precursor has been established as a key factor which controls the morphology of nanostructures obtained, it is natural to think that different titanium precursors, under the same reaction conditions, will undergo hydrolysis at different rates leading to different growth kinetics. To study the effect of different titanium precursors, we carried out growth using titanium isopropoxide (Ti-iPr) and titanium n-butoxide (Ti-iBu) in addition to $TiCl_4$ as titanium source. For growth rate comparisons, only FTO substrates were used resulting in nanowires with similar morphology (vertical array). Depending upon the Ti-precursor used, nanowires of different lengths were obtained. Figure 4 shows the variation of growth rate with three different titanium precursors. Nanowires were grown on FTO substrates with 10 mL of DI water, 10 mL of HCl, and 1 mL of each precursor at 180 °C for different growth times. The results revealed that $TiCl_4$ led to the fastest growth of nanowires with the length reaching 8 μm for a growth time of 6 h (nanowire film could be easily peeled off at this stage as shown in the inset of Figure 4), whereas it was only 5.6 μm in case of titanium isopropoxide. This behavior can be understood in terms of the reactivity of these precursors with water. Titanium tetrachloride is known to have a faster hydrolysis rate than the other reagents, which results in accelerated growth of nanowires because of faster supply of titanium growth units. Also, the diameter of nanowires grown

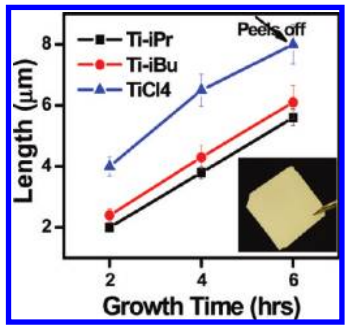

Figure 4. Effect of titanium precursor on the growth rate of nanowires. Variation of nanowire length with the growth time using 1 mL of $TiCl_4$, Ti-isopropoxide, and Ti-butoxide precursors each and with 10 mL of DI water and 10 mL of HCl at 180 °C on FTO substrates. The inset shows a photoimage of a nanowire film peeled off from the FTO substrate after a growth time of 8 h.

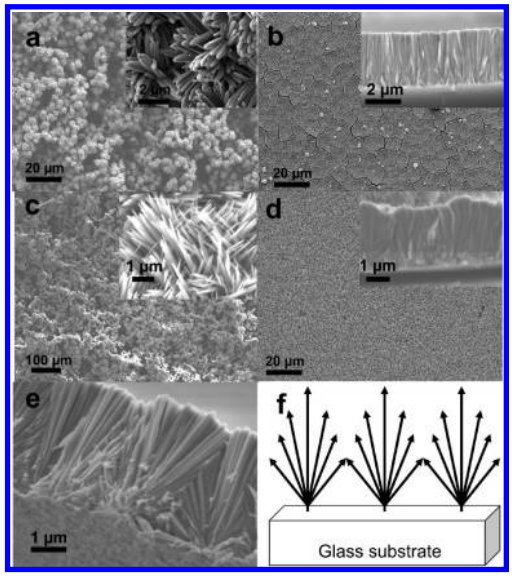

Figure 5. Effect of substrate positioning on the alignment of nanowires grown at 180 °C for 2 h using 1 mL of Ti-isopropoxide. SEM image of TiO_2 nanowires grown on (a) FTO substrate placed horizontally, (b) FTO substrate placed vertically, (c) glass substrate placed horizontally, and (d) glass substrate placed vertically. The main panel shows the top view SEM image, and the inset shows perspective and cross-sectional views. (e) High-resolution SEM of nanowire cross section grown on glass substrate and (f) schematic diagram showing the growth evolution of nanowires.

using $TiCl_4$ precursor was slightly larger (~100 nm) than those grown using titanium isopropoxide and titanium butoxide precursors (~80 nm).

Having discussed the effects of precursors on the growth kinetics, we have also observed very interesting effects of the substrate positioning inside the autoclave on the alignment of nanowires both on FTO and glass substrates. When the FTO substrate was placed horizontally with respect to the base of the autoclave, dandelion-shaped structures were obtained (Figure 5a) similar to those obtained on other substrates (e.g., Figure 1). On the other hand, when the substrate was placed vertically (or at a slight angle with FTO side facing down), a very nice vertically aligned array was obtained (Figure 5b). Similar growth behavior was observed in the case of glass substrate as well, namely, dandelion-shaped nanowires (Figure 5c) and an aligned array (Figure 5d) of nanowires were obtained when the glass substrate was loaded horizontally and vertically, respectively. We believe that when the substrate is placed horizontally, there is deposition of particles on the surface, and the particles act as

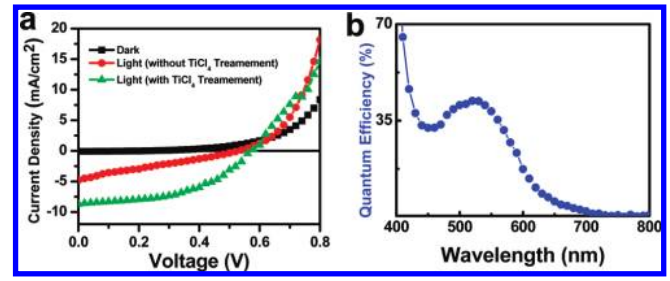

Figure 6. (a) $J-V$ characteristics of a dye-sensitized solar cell assembled with FTO substrate covered with 3 μm long rutile TiO_2 nanowire film as anode and 20 nm Pt deposited FTO substrate as cathode. The red curve shows the device with as-synthesized nanowires (without further treatment) immersed in dye solution for 12 h, and the yellow curve represents the device with nanowires treated with $TiCl_4$ solution and immersed in dye solution for 24 h. (b) External quantum efficiency data for the device treated with $TiCl_4$.

nucleating centers for further growth of nanowires resulting in dandelion-shaped structures. On the other hand, when the substrate is placed vertically, there is very little chance of reaction byproduct depositing on the surface thus promoting the growth of vertical nanowires. A closer look at the film cross section revealed that nanowires initially emanate radially from the nucleation site (Figure 5e). Nanowires that grow inclined away from the substrate normal obstruct nanowires growing off-normal from the adjacent nucleating site. Therefore, it is only the nanowires that are normal to the substrate that grow unobstructed resulting in *c*-axis orientation for the films. This is illustrated schematically in Figure 5f. Although the alignment is not as good as that on FTO, nanowires on glass show a decent degree of alignment in the perpendicular direction. Similar effects on the nanowire orientation were observed for Si/SiO_2 substrate as well.

Device Fabrication. The as-synthesized TiO_2 nanowires would have significant potential for dye solar cell application. We employed an FTO substrate covered with 3 μm long nanowires as the photoanode in assembling a dye-sensitized solar cell (DSSC). The conductivity of the underlying FTO substrate remains unaffected during the hydrothermal synthesis of TiO_2 nanowires because of mild synthesis conditions used. Figure 6a shows the Current-Voltage ($J-V$) characteristics from a typical dye-sensitized solar cell. Under an AM 1.5G illumination, the cell exhibits a short-circuit current of 4.8 mA/cm^2 and an open-circuit voltage of 0.54 V with an overall power-conversion efficiency of 1.2%. Remarkably, the performance of the cell increased drastically when a $TiCl_4$ post-treatment was carried out on the nanowire anode and the sample was kept immersed in the dye solution for 24 h. While the open-circuit voltage increased only by 40 mV, the short circuit current density increased to 8.7 mA/cm^2 giving an overall power-conversion efficiency of 2.9%. In addition, the fill factor of the cell increased from 41% to 59% upon $TiCl_4$ treatment.

The effects of $TiCl_4$ treatment have been previously studied in detail by O'Regan et al.[39] $TiCl_4$ treatment not only enhances the fill factor of the cell by reducing shunt current (because of formation of a thin TiO_2 blocking layer) but also increases the roughness factor which leads to enhanced dye absorption. In our case, however, we believe that a 2-fold increment in the power-conversion efficiency is a result of combination of two effects, namely, $TiCl_4$ treatment (resulting in increased roughness and reduced shunt loss) and greater dye loading because of increased immersion time. The device exhibits an external quantum efficiency (EQE) of ~60% at the peak absorption of dye as shown in Figure 6b. On the basis of SEM analysis, a

nanowire on average has four sides of 2000 nm × 80 nm and a top side of 80 nm × 80 nm. The specific surface area of the nanowire array is estimated to be 11 ± 3 m^2 g^{-1} by using a weight density of 4.25 g/cm^3 for rutile TiO_2. Following the dye desorption analysis, a typical value of 78 $nmol/cm^2$ for the dye concentration was obtained for our 3 μm long nanowire sample, which is lower than the values reported for anatase TiO_2 particles, consistent with previous reports of dye adsorption studies on rutile and anatase TiO_2 particles.[40] We did not observe any shorted devices after assembling the cell for samples without $TiCl_4$ treatment, which suggests that there is a thin layer of TiO_2 layer deposited on the FTO substrate during the nanowire growth, which works as the barrier layer and which prevents the electrolyte solution from touching the bottom FTO substrate. Although our efficiency is below the highest reported efficiency values for TiO_2 nanoparticle film anodes because of much thinner TiO_2 layer and other device optimizations, it compares well with the recently reported efficiencies of devices made using rutile nanowire arrays.[30,31]

Summary

In summary, a general synthesis procedure for the growth of TiO_2 nanowires on virtually any substrate was demonstrated for the first time. A moderately high concentration of Ti-precursors under highly acidic environment was used to obtain the growth of TiO_2 nanowire assemblies on arbitrary substrates. Both vertical array and dandelion-shaped TiO_2 nanowire assemblies can be obtained on various substrates including FTO, glass, ITO, Si/SiO_2, Si(100), and Si(111) substrates. Different titanium precursors were found to influence the growth rate of nanowires, and the behavior was explained in terms of the reactivity of these precursors toward hydrolysis. Alignment of nanowires was observed to be critically dependent on the positioning of the substrate inside the autoclave. Finally, a dye-sensitized solar cell with a power conversion efficiency of 2.9 ± 0.2% was fabricated using TiO_2 nanowires on FTO as photoanode.

Acknowledgment. This material is based upon work supported as part of the Center for Energy Nanoscience and Technology (CENT), an Energy Frontier Research Center (EFRC) funded by the U.S. Department of Energy, Office of Science and Office of Basic Energy Sciences under award number DE-SC0001013. SEM measurements were performed at the Center of Microscopy and Microanalysis at the University of Southern California. TEM and SAED measurements were carried out at the Doheny Eye Institute core instrumentation facility at the health science campus of USC.

Supporting Information Available: Additional information on (1) TiO_2 nanowires grown on glass rods and glass tubes, (2) TiO_2 nanowires grown on Si(100) and Si(111) substrates, and (3) schematic diagram of rutile nanowire growth habit. This material is available free of charge via the Internet at http://pubs.acs.org.

References and Notes

(1) Shen, G.; Chen, P. C.; Ryu, K.; Zhou, C. *J. Mater. Chem.* **2009**, *19*, 828–839.
(2) Huang, M. H.; Mao, S.; Feick, H.; Yan, H. Q.; Wu, Y. Y.; King, H.; Weber, E.; Russo, R.; Yang, P. D. *Science* **2001**, *292*, 1897–1899.
(3) Pan, Z. W.; Dai, Z. R.; Wang, Z. L. *Science* **2001**, *291*, 1947.
(4) Greene, L. E.; Law, M.; Goldberger, J.; Kim, F.; Johnson, J. C.; Zhang, Y.; Saykally, R. J.; Yang, P. D. *Angew. Chem., Int. Ed.* **2003**, *42*, 3031–3034.
(5) Greene, L. E.; Law, M.; Tan, D. H.; Montano, M.; Goldberger, J.; Somorjai, G.; Yang, P. D. *Nano Lett.* **2005**, *5*, 1231–1236.
(6) Vayssieres, L.; Graetzel, M. *Angew. Chem., Int. Ed.* **2004**, *43*, 3666–3670.
(7) Baxter, J. B.; Aydil, E. S. *Appl. Phys. Lett.* **2005**, *86*, 053114.
(8) Tian, Z. R.; Voigv, J. A.; Liu, J.; Mckenzie, B.; Xu, H. F. *J. Am. Chem. Soc.* **2003**, *125*, 12384–12385.
(9) Mor, G. K.; Shankar, K.; Paulose, M.; Varghese, O. K.; Grimes, C. A. *Nano Lett.* **2006**, *6*, 215–218.
(10) Zhu, K.; Neale, N. R.; Miedaner, A.; Frank, A. J. *Nano Lett.* **2007**, *7*, 69–74.
(11) Yang, P. D.; Yan, H. Q.; Mao, S.; Russo, R.; Johnson, J.; Saykally, R.; Morris, N.; Pham, J.; He, R. R.; Cho, H. J. *Adv. Funct. Mater.* **2002**, *12*, 323.
(12) Pfaff, G.; Reynders, P. *Chem. Rev.* **1999**, *99*, 1963.
(13) Zallen, R.; Moret, M. P. *Solid State Commun.* **2006**, *137*, 154.
(14) Braun, J. H.; Baidins, A.; Marganski, R. E. *Prog. Org. Coat.* **1992**, *20*, 105.
(15) Salvador, A.; Pascual-Marti, M. C.; Adell, J. R.; Requeni, A.; March, J. G. *Pharm. Biomed. Anal.* **2000**, *22*, 301.
(16) Choi, W.; Termin, A.; Hoffman, M. R. *J. Phys. Chem.* **1994**, *98*, 13669.
(17) Yuhas, B. D.; Zitoun, D. O.; Pauzauski, P. J.; He, R.; Yand, P. D. *Angew. Chem., Int. Ed.* **2006**, *45*, 420.
(18) O'Regan, B.; Gratzel, M. *Nature* **1991**, *353*, 737.
(19) Mor, G. K.; Shankar, K.; Paulose, M.; Varghese, O. K.; Grimes, C. A. *Nano Lett.* **2006**, *6*, 215.
(20) Kongkanand, A.; Tvrdy, K.; Takechi, K.; Kuno, M. K.; Kamat, P. V. *J. Am. Chem. Soc.* **2008**, *130*, 4007.
(21) Fujishima, A.; Honda, K. *Nature* **1972**, *37*, 238.
(22) Chae, S. Y.; Park, M. K.; Lee, S. K.; Kim, T. Y.; Kim, S. K.; Lee, W. I. *Chem. Mater.* **2003**, *15*, 3326.
(23) Greene, L. E.; Law, M.; Goldberger, J.; Kim, F.; Johnson, J. C.; Zhang, Y.; Saykally, R. J.; Yang, P. D. *Angew. Chem., Int. Ed.* **2003**, *42*, 3031–3034.
(24) Greene, L. E.; Yuhas, B. D.; Law, M.; Zitoun, D.; Yang, P. D. *Inorg. Chem.* **2006**, *45*, 7535–7543.
(25) Weng, C.-C.; Hsu, K.-F.; Wei, K.-H. *Chem. Mater.* **2004**, *16*, 4080–4086.
(26) Hosono, E.; Fujihara, S.; Kakiuchi, K.; Imai, H. *J. Am. Chem. Soc.* **2004**, *126*, 7790–7791.
(27) Chen, C. A.; Chen, Y. M.; Korotcov, A.; Huang, Y. S.; Tsai, D. S.; Tiong, K. K. *Nanotechnology* **2008**, *19*, 075611.
(28) Prakasam, H. E.; Shankar, K.; Paulose, M.; Varghese, O. K.; Grimes, C. A. *J. Phys. Chem. C* **2007**, *111*, 7235.
(29) He, Y. P.; Zhang, Z. Y.; Zhao, Y. P. *J. Vac. Sci. Technol., B* **2008**, *26*, 1350.
(30) Liu, B.; Aydil, E. S. *J. Am. Chem. Soc.* **2009**, *131*, 3985.
(31) Feng, X.; Shankar, K.; Varghese, O. K.; Paulose, M.; Latempa, T. J.; Grimes, C. A. *Nano Lett.* **2008**, *8*, 3781.
(32) Chhabra, V.; Pillai, V.; Mishra, B. K.; Morrone, A.; Shah, D. O. *Langmuir* **1995**, *11*, 307.
(33) Wu, M.; Long, J.; Huang, A.; Luo, Y. *Langmuir* **1999**, *15*, 8822.
(34) Chu, R.; Yan, J.; Lian, S.; Wang, Y.; Yan, F.; Chen, D. *Solid State Commun.* **2004**, *130*, 789.
(35) Allen, P. B. *Nano Lett.* **2007**, *7*, 6.
(36) Howard, W. J. *Crystal Chemistry and Refractivity*; Cambridge University Press: Cambridge, U.K., 1988.
(37) Wells, A. F. *Structural Inorganic Chemistry*, 4th ed.; Clarendon Press: Oxford, U.K., 1975.
(38) Cheng, H.; Ma, J.; Zhao, Z.; Qi, L. *Chem. Mater.* **1995**, *7*, 66.
(39) O'Regan, B. C.; Durrant, J. R.; Sommeling, P. M.; Bakker, N. J. *J. Phys. Chem. C* **2007**, *111*, 14001.
(40) Park, N.-G.; van de Lagemaat, J.; Frank, A. J. *J. Phys. Chem. B* **2000**, *104*, 8989.

JP100491H